

Helical Superstructure of Intermediate Filaments

Lila Bouzar,¹ Martin Michael Müller,^{2,3} René Messina,² Bernd Nöding,⁴ Sarah Köster,⁴

Hervé Mohrbach,^{2,3} and Igor M. Kulić^{3,*}

¹Laboratoire de Physique des Matériaux, USTHB, BP 32 El-Alia Bab-Ezzouar, 16111 Alger, Algeria

²Laboratoire de Physique et Chimie Théoriques—UMR 7019, Université de Lorraine, 1 boulevard Arago, 57070 Metz, France

³Institut Charles Sadron, CNRS-UdS, 23 rue du Loess, BP 84047, 67034 Strasbourg cedex 2, France

⁴Institute for X-Ray Physics, University of Goettingen, Friedrich-Hund-Platz 1, 37077 Göttingen, Germany



(Received 13 March 2018; published 6 March 2019)

Intermediate filaments are the least explored among the large cytoskeletal elements. We show here that they display conformational anomalies in narrow microfluidic channels. Their unusual behavior can be understood as the consequence of a previously undetected, large-scale helically curved superstructure. Confinement in a channel orders the otherwise soft, strongly fluctuating helical filaments and enhances their structural correlations, giving rise to experimentally detectable, strongly oscillating tangent correlation functions. We propose an explanation for the detected intrinsic curving phenomenon—an elastic shape instability that we call autocoining. The mechanism involves self-induced filament buckling via a surface stress located at the outside of the cross section. The results agree with ultrastructural findings and rationalize for the commonly observed looped intermediate filament shapes. Beyond curvature, explaining the molecular origin of the detected helical torsion remains an interesting challenge.

DOI: 10.1103/PhysRevLett.122.098101

The integrity and dynamics of biological cells delicately depend on the mechanical response of their cytoskeleton consisting of actin filaments, microtubules, and intermediate filaments (IFs) [1,2]. While they have been experimentally probed in many different ways, a full understanding of their properties still remains a challenge. This is particularly true for the IFs—the least studied. Experiments probing their elastic response have shown that they are the most flexible and extensible of the filaments of the cytoskeleton [3–6]. Biofilaments are usually modeled as semiflexible polymers characterized by their persistence length. For vimentin, a prominent member of the IF family, this model was used in combination with various experimental methods to determine values for the persistence length of a few microns [3,7,8].

In most of the experiments, the IFs interact strongly with a substrate (in atomic force and electron microscopy), and the extracted physical properties depend on the substrate properties the filaments adhere to. A closer look at the experimental micrographs [3,7,8] reveals shapes that resemble sinusoidal waves, loops, or circular arcs reminiscent of helices confined to a 2D substrate [9,10]. This leads to the suspicion that IFs are not simple enough to be described by a semiflexible chain. To eliminate possible artifacts from adsorption, we have studied individual IFs in quasi-two-dimensional microfluidic channels where the filaments, despite geometric confinement, are free to rearrange. Averaging over a number of different filaments, a persistence length close to 2 μm was found previously [11]. However, a deeper inspection of the *individual*

filament data, that we will present in this Letter, reveals an anomalous behavior which is incongruent with the expected behavior of a semiflexible polymer. For instance, we observe the transient formation of rings and oscillatory shapes (see Fig. 1 and Supplemental videos [12]). However, the most prominent manifestation of this anomaly is found in a strongly oscillating tangent correlation function for individual filaments, in sharp contrast to the behavior characteristic for a semiflexible chain under lateral confinement [13]. In this Letter, we will show that the data can be completely rationalized by assuming that IFs behave like squeezed helical filaments under lateral confinement.

A central observable in our study is the tangent correlation function $G(s)$ that provides crucial conformational information about the filament's microstructure. More specifically, it is defined as

$$G(s) = \overline{\langle \cos \phi(s) \rangle}, \quad (1)$$

where $\phi(s)$ is the tangent angle of the filament at the arclength position s ; see the sketch in Fig. 1(b). $\langle \dots \rangle$ in Eq. (1) denotes thermal average and $\overline{\langle \dots \rangle}$ the spatial average along the contour length (L), i.e., $f[\overline{\langle \phi(s) \rangle}] = [1/(L-s)] \int_0^{L-s} du f[\phi(u+s) - \phi(u)]$; see also Fig. 1(b).

Revisited (unpublished) experimental data on vimentin filaments whose setup is described in detail elsewhere [11] are displayed in Fig. 2. Quasi-two-dimensional microfluidic channels of height h and varying lateral confinement d were employed to confine these filaments. Upon limiting

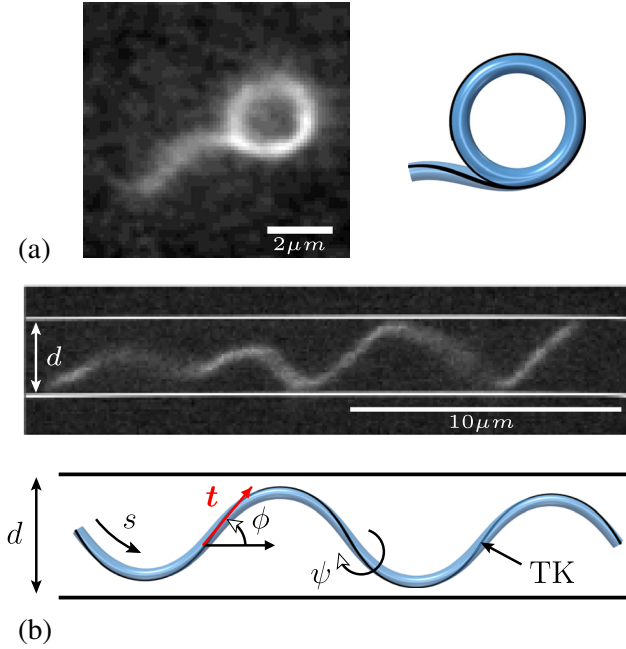


FIG. 1. (a) Left panel: Vimentin filament confined in a slit occasionally coiled up in a transient ring; see Supplemental Material [12], Video 3. Right panel: Model three-dimensional helical filament getting confined to a plane forming a ring as an energy minimum; see Eq. (2) and the text. (b) Upper panel: Typical oscillatory shape of an intermediate filament in a quasi-two-dimensional microfluidic channel characterized by a lateral confinement d [11]; see Supplemental Videos 1 and 2 [12]. Lower panel: Geometrical setup of the model filament. The tangent vector t evolves with arclength s along the filament. Its direction is given by the angle $\phi(s)$, measured from the horizontal. $\psi(s)$ denotes the twist angle represented by a black ribbon on the filament's surface. The variation of the twist at curvature inversion points gives rise to conformational defects called twist kinks (TKs).

the thermal average of $\overline{\cos \phi(s)}$ to an *individual* filament, striking oscillations in $G(s)$ set in; see Fig. 2. At a prescribed height ($h = 0.45 \mu\text{m}$), the two profiles in the main body in Fig. 2 (red and yellow symbols) correspond to two different lateral confinements ($d = 1.6 \mu\text{m}$ and $d = 2.7 \mu\text{m}$). $G(s)$ increases with decreasing d (i.e., with an increasing degree of lateral confinement) as expected, whereas the oscillation amplitudes as well as their associated wavelength decrease. These features remain robust upon changing the channel height to $1 \mu\text{m}$; see the green circles in the inset in Fig. 2.

In the following, we rationalize these observations by means of Monte Carlo (MC) simulations as well as the analytical theory. The underlying idea is that confined IFs can be modeled as a helical superstructure trapped on a flat surface and subject to an additional lateral confinement.

Consider a helical Euler-Kirchhoff filament of length L , characterized by Euler angles ψ , ϕ , and θ [14]. Flattening the filament onto a plane constrains the third angle to $\theta = \pi/2$, and its elastic energy is given by [9,10]

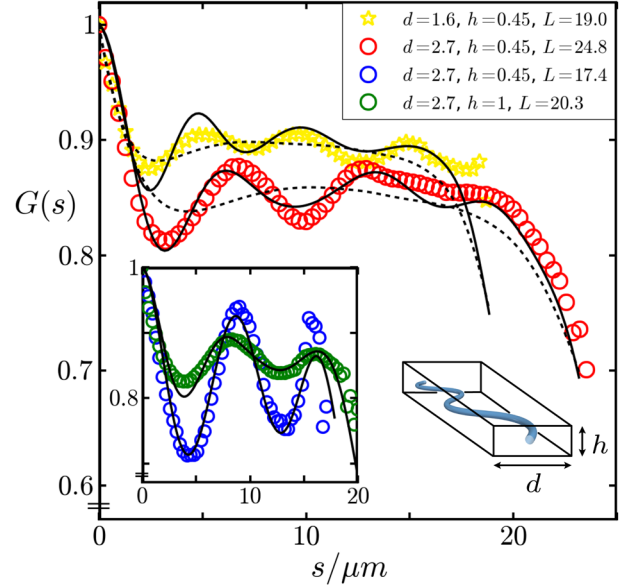


FIG. 2. Tangent correlation functions $G(s)$ of vimentin filaments (experimental data represented by symbols) confined in a quasi-two-dimensional microfluidic channel of width d and height h given in microns (as well as L); see the bottom right inset. Bottom left inset: (i) Data for $h = 1 \mu\text{m}$ (green circles). (ii) Sample exhibiting strong and persisting oscillations in $G(s)$ (blue circles). Solid (dashed) lines stem from MC simulation data of filaments in two dimensions (i.e., $h = 0$) with (without) twist.

$$E = \frac{1}{2} \int_0^L [B(\phi' - \omega_1 \sin \psi)^2 + C(\psi' - \omega_3)^2 + B\omega_1^2 \cos^2 \psi] ds, \quad (2)$$

where $\phi'(s) =: \kappa(s)$ stands for the curvature, ψ designates the twist angle, and $\psi'(s)$ is the twist with s being the arclength; see also Fig. 1(b). The constants B and C in Eq. (2) are the bending and torsional stiffness, respectively, and ω_1 and ω_3 are the preferred curvature and twist, respectively, of the unconfined three-dimensional helical filament [15].

The filament ground state stemming from Eq. (2) obeys two coupled equations: the pendulumlike equation (i) $\psi'' + [(B\omega_1^2)/(2C)] \sin(2\psi) = 0$ and (ii) $\kappa = \omega_1 \sin \psi$ indicating that curvature is slaved by the twist angle in contrast to the unconfined three-dimensional case (where both decouple). In general, depending on the material parameters, a rich variety of equilibrium shapes resembling loops, waves, spirals, or circles exist [10]. These shapes can be seen as the result of interacting repulsive conformational defects corresponding to curvature inversion points. In terms of twist, such defects originate from a rapid variation of $\psi(s)$ (reminiscent of a kink) and are called twist kinks (TKs). A relevant dimensionless parameter is $\gamma = (4\omega_1^2 B / \pi^2 \omega_3^2 C)$, which measures the ratio of bending and twisting energy. For $\gamma > 1$, the ground state approaches a TK-free circular arc of radius $1/\omega_1$; see Fig. 1(a).

For $\gamma < 1$, the filament can be populated by TKs whose density is limited by their repulsion [16].

Extensive MC simulations based on the Hamiltonian in Eq. (2) have been carried out to explore the conformations of confined filaments in full detail; see Supplemental Material, Sec. S2 [12]. Our best matching MC data for $G(s)$ can be found in Fig. 2. Interestingly, taking into account the twist via Eq. (2) corroborates the experimentally observed oscillations by employing consistent material parameters [17]; see Fig. 2. These results suggest that the unconfined vimentin possesses a helical superstructure characterized by a radius $\sim 0.4 \mu\text{m}$ and pitch $\sim 4 \mu\text{m}$ and a bending persistence length $B/(k_B T) \sim 50 \mu\text{m}$ [18]. In contrast, for straight semiflexible chains, no oscillations emerge in $G(s)$ where the usual Odijk behavior [13] is recovered; see the dashed lines in Fig. 2.

To deepen our understanding of the role of the internal twist, that is a hidden degree of freedom in the experiments, we analyze the simulated filament conformation for various degrees of lateral confinement. A useful quantity is the probability density of TK occurrence, $p(n)$, where n is the number of TKs which is adequately defined as $n = (1/\pi) \int_0^L \psi'(s) ds$. Probability density profiles $p(n)$ for varying lateral confinement d are depicted in Fig. 3(a). On average, the number of TKs increases with decreasing d ; see Fig. 3(a). Computing the corresponding $G(s)$ (not shown) clearly indicates that the average number of TKs n also describes the number of extrema encountered in $G(s)$. Thermal fluctuations induce injections and ejections of TKs at the ends of the filament, which qualitatively explains the fading of the oscillations in $G(s)$ shown in Fig. 2. Dynamic TK number switching is also observed experimentally; see Supplemental Fig. 1 [12].

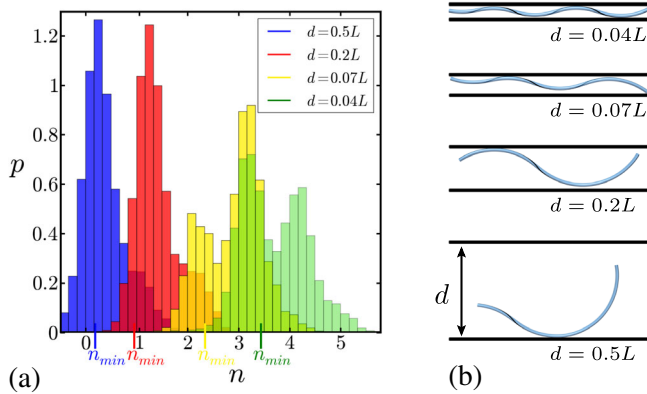


FIG. 3. (a) Simulation data for the probability density of the number of TKs n for different values of the lateral confinement d with $\omega_1 = \pi$, $\gamma = 5$, $B = 10$, and $C = 0.16$ (with $k_B T = L = 1$). (b) Low-temperature snapshots of a filament close to its ground state for the same values of d as in the histogram illustrating the TK injection.

To shed more light on the underlying physical mechanisms of confinement-mediated TK production, let us consider a more tractable analytical model. It consists in replacing the confinement by a pulling force at zero temperature; see Fig. 4. In the presence of the external force F and for small deformations ($\varphi \ll 1$), the elastic energy becomes

$$E_F \simeq E + \frac{F}{2} \int_0^L \phi^2(s) ds. \quad (3)$$

Consider the regime $\gamma \gg 1$ which has as a ground state (in the absence of a force) a circular arc $\phi(s) = -\omega_1 s$ and energy $E_0 = CL\omega_1^2/2$; see Fig. 4. The formation of a TK is energetically favorable when the pulling force exceeds a critical value $F_c = (64/L^3\omega_1)\sqrt{BC}$. The latter is the result of a comparison of the elastic energy of a TK-free filament ($E_0 + (\omega_1^2 L^3/24)F$) with that of a filament containing a single TK located at the midpoint ($E_0 + \omega_1\sqrt{BC} + (\omega_1^2 L^3/96)F$); see Fig. 4. In the opposite, small force regime ($F < F_c$), the filament deforms like a stretched elastic arc; see Fig. 4.

Above F_c , one or more TKs are formed; see Fig. 4. The required force to nucleate n TKs is given by $F_c(n) = [(48\sqrt{BC})/(L^3\omega_1)]\{[n^2(n+1)^2]/(2n+1)\}$. Note that the kinks mutually repel each other, giving rise to an ordered one-dimensional crystal-like structure of n TKs separated by circular arcs of switching curvature; see Fig. 4.

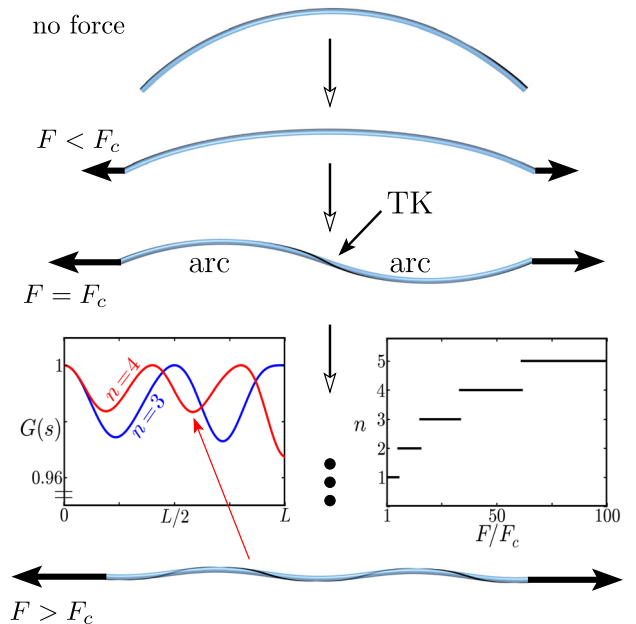


FIG. 4. Evolution of a ground state of an elastic filament with curvature under an external pulling force. Inset (left): Corresponding tangent correlation functions for $n = 3$ (blue) and $n = 4$ (red) TKs. Inset (right): The number of twist kinks as a function of the tension.

Expanding the chain conformation in Fourier modes and keeping only the dominant one, we extract the tangent correlation function:

$$G(s) \approx 1 - \frac{16\ell^2\omega_1^2}{\pi^4} \sin^2\left(\frac{\pi s}{2\ell}\right) \left(1 + \frac{\ell \sin(\pi s/\ell)}{\pi(L-s)}\right) \quad (4)$$

with $\ell = L/(n+1)$ representing the distance between two adjacent TKs. Typical profiles of $G(s)$, displaying oscillations similar to the confinement case, are shown in Fig. 4. Simulation results with external force, not shown here, corroborate these findings.

Thus, our results strongly suggest that vimentin filaments have a helical superstructure of a yet unclear origin. Oscillations in the tangent correlation functions of individual actin filaments were also previously observed [19,20] and helical superstructures of microtubule reported [21,22]. Therefore, the natural question of a more general physical mechanism arises. Here we propose a model based on self-buckling, for which we suggest the name *autocoiling*; see Fig. 5. It is generic for filaments exposed to surface stresses that induce a broken symmetry via curved states and can be witnessed in the mundane example of drying spaghetti; see Fig. 5(c). The outer layer of the spaghetti dries and shrinks faster and induces a buckling stress on the (transiently) more swollen core.

For vimentin, there are several hints towards a surface stress from its molecular structure. During the assembly of vimentin monomers, they form highly elongated coiled-coil dimers and then tetramers and at an intermediate stage give rise to an approximately “spindle-shaped” 32-mer (see images in Ref. [23])—the so-called unit length filament (ULF) [24]. These ULFs then assemble into long filaments. The initially rugged, “rough” filaments of spindle-like ULF subunits longitudinally anneal, and the filaments undergo a maturation phase during which the surface smoothen [23,24]. We suggest that the spindle shape and the finite lateral thickness of the ULF can be understood as originating from double-twist frustration caused by chiral (cholesteric) interactions of the coiled-coil alpha helices aligned along the axis. As proposed in Ref. [25], a bundle

of chiral objects displays a finite size, as the chains on the outside are progressively more tilted than those on the inside. This tilt causes a surface stress and axial shortening of the outer chains with respect to the inner ones.

As the simplest possible model for self-buckling under a surface stress, we consider an isotropic incompressible elastic rod of radius R and length L . Its energy is $U = \frac{1}{2} \int dV \sigma_{ij} \varepsilon_{ij} + \lambda \Delta S$, where σ_{ij} and ε_{ij} are the bulk stress and strain tensor, respectively. The constant $\lambda > 0$ is an isotropic tensile surface stress (surface energy density). ΔS denotes the variation of the surface after deformation. When negative, the term $\lambda \Delta S$ can compete with the positive elastic bulk energy. Under a pure bending deformation with a constant curvature κ of the rod, the cross section is slightly deformed [see Fig. 5(a)], and $\Delta S < 0$ as deduced from the deformation field of a bent rod [26]. It can be shown that $(\Delta S/S_0) \approx -\frac{3}{16} R^2 \kappa^2$, where $S_0 = 2\pi LR$ is the surface of the undeformed rod. The total surface + elastic energy can then be written as $U = \frac{1}{2} B_e(\lambda) L \kappa^2$ with an effective bending modulus that has contributions from both the bulk and the surface stress of the rod: $B_e(\lambda) = (\pi/4) Y R^4 - \lambda (3\pi/4) R^3$, where Y is the Young modulus. For sufficiently large λ , the stiffness $B_e(\lambda)$ vanishes and the rod becomes unstable. This is the signature of a spontaneous broken symmetry of the rod, i.e., self-buckling [27].

Beyond the curvature, the precise molecular origin of the helical torsion of vimentin remains currently unexplained and calls for further investigation. At this point, we might speculate that the handedness and pitch are inherited from the chiral inter-alpha-helix interaction on the monomer level and bear some similarity to bacterial flagella [28] and microtubule superhelical states [21,22].

In summary, we report evidence for a helical superstructure in intermediate filaments. Lateral confinement in a quasi-2D channel orders the otherwise soft and strongly fluctuating TK defects and leads to experimentally detectable, oscillating tangent correlation functions. The underlying physical mechanism is the injection of low-energy defects, that can be seen as a new deformation mode for confined helical filaments. This behavior is reminiscent of the plastic deformations mediated by dislocations in solids [29]. The self-buckling mechanism suggested to be at the origin of the curved states of vimentin could also be common in other biological filaments beyond IFs. More generally, tensile surface stress could be induced by any mismatch between the surface and the bulk of the filament, like, e.g., the surface tension between the ordered water and ions at the outer layers of the filament that display mismatched osmotic and Maxwell stresses between the interior and exterior.

The biological meaning of an intrinsically stiffer but coiled helical structure is apparent. A coiled structure resists small forces by uncoiling and displays high compliance without damage up to the point of stronger elongation. This reinforces the IFs’ natural role as supporting mechanical elements and protective stress absorbers of the cell.

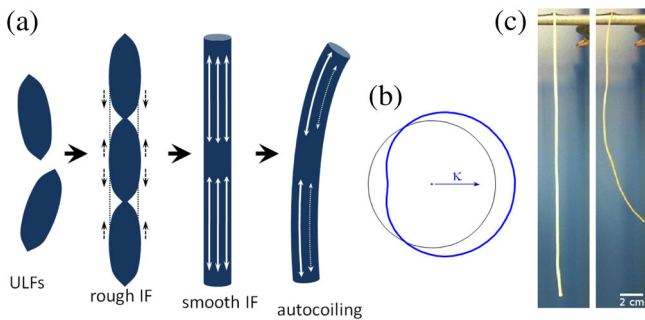


FIG. 5. (a) Stages of assembly of IFs and their autocoiling instability. (b) The cross-section deformation of the bent circular rod. (c) The autocoiling of drying spaghetti.

*Corresponding author.

kulic@unistra.fr

- [1] B. Alberts *et al.*, *Molecular Biology of the Cell*, 4th ed. (Garland Science, New York, 2002).
- [2] A. Amos and W. G. Amos, *Molecules of the Cytoskeleton* (Guilford, New York, 1991).
- [3] N. Mücke, L. Kreplak, R. Kirmse, T. Wedig, H. Herrmann, U. Aebi, and J. Langowski, Assessing the flexibility of intermediate filaments by atomic force microscopy, *J. Mol. Biol.* **335**, 1241 (2004).
- [4] L. Kreplak, H. Bär, J. F. Leterrier, H. Herrmann, and U. Aebi, Exploring the mechanical behavior of single intermediate filaments, *J. Mol. Biol.* **354**, 569 (2005).
- [5] L. Kreplak, H. Herrmann, and U. Aebi, Tensile properties of single desmin intermediate filaments, *Biophys. J.* **94**, 2790 (2008).
- [6] J. Block, H. Witt, A. Candelli, E. J. G. Peterman, G. J. L. Wuite, A. Janshoff, and S. Köster, Nonlinear Loading-Rate-Dependent Force Response of Individual Vimentin Intermediate Filaments to Applied Strain, *Phys. Rev. Lett.* **118**, 048101 (2017).
- [7] S. Winheim, A. R. Hieb, M. Silbermann, E.-M. Surmann, T. Wedig, H. Herrmann, J. Langowski, N. Mücke, and L. Kreplak, Deconstructing the late phase of vimentin assembly by total internal reflection fluorescence microscopy (TIRFM), *PLoS One* **6**, e19202 (2011).
- [8] M. Schopferer, H. Bär, B. Hochstein, S. Sharma, N. Mücke, H. Herrmann, and N. Willenbacher, Desmin and vimentin intermediate filament networks: Their viscoelastic properties investigated by mechanical rheometry, *J. Mol. Biol.* **388**, 133 (2009).
- [9] G.-M. Nam, N.-K. Lee, H. Mohrbach, A. Johnner, and I. M. Kulić, Helices at interfaces, *Europhys. Lett.* **100**, 28001 (2012).
- [10] L. Bouzar, M. M. Müller, P. Gosselin, I. M. Kulić, and H. M. Mohrbach, Squeezed helical elastica, *Eur. Phys. J. E* **39**, 114 (2016).
- [11] B. Nöding and Sarah Köster, Intermediate Filaments in Small Configuration Spaces, *Phys. Rev. Lett.* **108**, 088101 (2012).
- [12] See Supplemental Material at <http://link.aps.org/supplemental/10.1103/PhysRevLett.122.098101> for additional derivations, figures and videos.
- [13] T. Odijk, The statistics and dynamics of confined or entangled stiff polymers, *Macromolecules* **16**, 1340 (1983).
- [14] M. Nizette and A. Goriely, Towards a classification of Euler–Kirchhoff filaments, *J. Math. Phys. (N.Y.)* **40**, 2830 (1999).
- [15] N. Chouaieb, A. Goriely, and J. H. Maddocks, Helices, *Proc. Natl. Acad. Sci. U.S.A.* **103**, 9398 (2006).
- [16] Note that, while both kinks ($\psi' > 0$) and antikinks ($\psi' < 0$) are possible, one of the two is energetically unfavorable in the presence of the intrinsic twist term. For $\omega_3 > 0$ ($\omega_3 < 0$), only the kinks (antikinks) are stable.
- [17] (i) For simulation data with finite twist, the elastic constants are $B/(k_B T) \simeq 50 \mu\text{m}$ and $C/(k_B T) \simeq 3 \mu\text{m}$, except for the corresponding experimental data with blue circles where $C/(k_B T) \simeq 10 \mu\text{m}$. The geometrical parameters are typically $\omega_1^{-1} \simeq 2 \mu\text{m}$ or $\omega_3^{-1} \simeq 1 \mu\text{m}$. (ii) For twist-free filaments (i.e., $\omega_1 = \omega_3 = C = 0$), $B/(k_B T) \simeq 5 \mu\text{m}$.
- [18] Note that the value of B is much higher than determined previously from multifilament averaging—a procedure that neglects single filament correlations and measures an “apparent” persistence length.
- [19] S. Köster, J. Kierfeld, and T. Pfohl, Characterization of single semiflexible filaments under geometric constraints, *Eur. Phys. J. E* **25**, 439 (2008).
- [20] S. Köster, D. Steinhauser, and T. Pfohl, Brownian motion of actin filaments in confining microchannels, *J. Phys. Condens. Matter* **17**, S4091 (2005).
- [21] H. Mohrbach, A. Johnner, and I. M. Kulić, Tubulin Bistability and Polymorphic, Dynamics of Microtubules, *Phys. Rev. Lett.* **105**, 268102 (2010).
- [22] H. Mohrbach, A. Johnner, and I. M. Kulić, Cooperative lattice dynamics and anomalous fluctuations of microtubules, *Eur. Biophys. J.* **41**, 217 (2012).
- [23] H. Herrmann, M. Häner, M. Brettel, N.-O. Ku, and U. Aebi, Characterization of distinct early assembly units of different intermediate filament proteins, *J. Mol. Biol.* **286**, 1403 (1999).
- [24] H. Herrmann and U. Aebi, Intermediate filaments: Molecular structure, assembly mechanism, and integration into functionally distinct intracellular scaffolds, *Annu. Rev. Biochem.* **73**, 749 (2004).
- [25] G. M. Grason and R. F. Bruinsma, Chirality and Equilibrium Biopolymer Bundles, *Phys. Rev. Lett.* **99**, 098101 (2007).
- [26] W. M. Lai, D. Rubin, and E. Kreml, *Introduction to Continuum Mechanics* (Elsevier, New York, 2010).
- [27] The autocooling instability gives rise to a zero elastic energy mode [30] and a free energy that depends only on the magnitude of curvature and not on its direction, displaying a continuously degenerated ground state in contrast to Eq. (2). However, it can be shown that the Euler–Kirchhoff beam model, Eq. (2), is approximately valid in the absence of end attachment of the filament and when the angular phase of the “polymorphic” curvature (with respect to the material frame) is not directly observable [21,22].
- [28] C. R. Calladine, Construction of bacterial flagella, *Nature (London)* **255**, 121 (1975).
- [29] J. Friedel, R. Smoluchowski, and N. Kurti, *Dislocations*, International Series of Monographs on Solid State Physics (Pergamon Press, Oxford, 1964).
- [30] A. Baumann, A. Sánchez-Ferrer, L. Jacomine, P. Martinoty, V. Le Houerou, F. Ziebert, and I. M. Kulić, Motorizing fibres with geometric zero-energy modes, *Nat. Mater.* **17**, 523 (2018).